A Rigorous Analysis of a Coaxial to Shielded Microstrip Line Transition

CHRISTOS N. CAPSALIS, CONSTANTINOS P. CHRONOPOULOS, AND NIKOLAOS K. UZUNOGLU, MEMBER, IEEE

Abstract—**The transition from a coaxial to a shielded microstrip line is analyzed by applying a rigorous mode-matching technique. The symmetry axes of the two transmission lines are assumed to be parallel while the relative position of the coaxial line center conductor with respect to the microstrip line is taken to be arbitrary. The fields inside the shielded microstrip line are expanded in terms of the normal hybrid modes, while in describing the fields inside the coaxial line the transverse electric and magnetic modes are utilized. Both propagating and evanescent modes are taken into account in each transmission line. A modified mode-matching procedure is employed on the junction plane of the two transmission lines to formulate the corresponding discontinuity problem. The mode-matching equations are solved by applying projection techniques. Numerical stability and computational efficiency are achieved in determining the scattering parameters of the coaxial to microstrip line transitions. Numerical results are computed and presented for several coaxial to microstrip line transition geometries.**

I. INTRODUCTION

COAXIAL AND microstrip lines are the most common waveguides used in transmitting low-power microwave and low-frequency millimeter-wave signals. In many instances there is a need to join these two types of transmission lines.

The natural way to connect shielded microstrip to coaxial line is to join the two inner and outer conductors directly. However, it is clear from the beginning that the transition from the "cylindrical" coaxial structure to the "planar rectangular" microstrip would present quite a strong discontinuity. As a result, standing waves and insertion losses will be present in these types of junctions. It is expected that the use of such transitions in the 20–60 GHz band region will address quite important practical problems in comparison with conventional microwave frequencies, where the transition problems are less severe. The reflection at the transition of a coaxial line to a stripline has been considered by Schminke [1] by assuming an intermediate "Zwischenmedium" rectangular waveguide region between the two lines. Also, empirical methods have been proposed to solve the problem of coaxial to microstrip transition [2]. A compensation technique has been proposed by England [3] to reduce the reflection coefficient.

Manuscript received March 23, 1988; revised February 3, 1989.

The authors are with the Department of Electrical Engineering, National Technical University of Athens, Athens 10682, Greece.

IEEE Log Number 8927797.

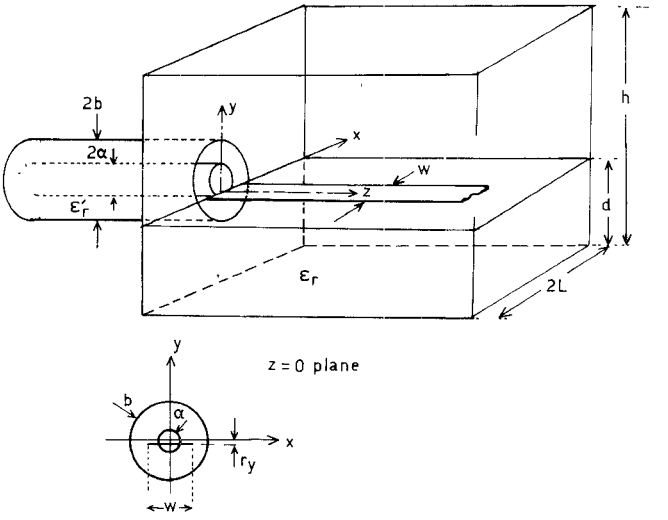

Fig. 1. Coaxial to shielded microstrip transition geometry.

In this paper a rigorous analysis is developed to analyze the coaxial line to microstrip transition by taking into account all the geometrical details pertaining to this structure.

The geometry of the coaxial to microstrip line transition is shown in Fig. 1. The two transmission lines join each other on the $z = 0$ plane. The shielding box height and width of the microstrip line are denoted by h and $2L$, respectively, while the substrate permittivity and thickness are ϵ_r and d, respectively. The printed microstrip line width is indicated by w. The coaxial line dimensions are defined in terms of the inner and outer radii a and b shown in Fig. 1 and the permittivity ϵ_r' of the dielectric material filling the region between two conductors. The transition is assumed to preserve the y symmetry in the $z = 0$ junction plane while the displacement of the coaxial line axis from the printed microstrip line axis is indicated by r_y (see Fig. 1). The microstrip shielding box dimensions are sufficiently large so that on the $z = 0$ transition plane the coaxial line boundaries are always inscribed inside the rectangular shielding box as shown in Fig. 1. Furthermore on the $z = 0$ junction plane the nonoverlapping regions of

0018-9480/89/0700-1091$01.00

TABLE I
COAXIAL LINE MODE PROPERTIES

	TE	TM	TEM
Longitudinal Component	$H_z = h^{TE}_{z,mn}(\rho,\varphi)e^{-\gamma'_{mn}z}$ $h^{TE}_{z,mn}(\rho,\varphi) = (J_m(h'_{mn}\rho) - \frac{J'_m(h'_{mn}\alpha)}{Y'_m(h'_{mn}\alpha)} Y_m(h'_{mn}\rho))$ $\cdot\begin{cases}\sin(m\varphi) & \text{for } m=2,4,6,\ldots\\ \cos(m\varphi) & \text{for } m=1,3,5,\ldots\end{cases}$	$E_z = e^{TM}_{z,mn}(\rho,\varphi)e^{-\gamma_{mn}z}$ $e^{TM}_{z,mn}(\rho,\varphi) = (J_m(h_{mn}\rho) - \frac{J_m(h_{mn}\alpha)}{Y_m(h_{mn}\alpha)} Y_m(h_{mn}\rho))$ $\cdot\begin{cases}\cos(m\varphi) & \text{for } m=0,2,4.,\\ \sin(m\varphi) & \text{for } m=1,3,5,.\end{cases}$	
Propagation condition	$J'_m(h'_{mn}\alpha)Y'_m(h'_{mn}b) - Y'_m(h'_{mn}\alpha)J'_m(h'_{mn}b) = 0$ $\gamma'^2_{mn} = h'^2_{mn} - \omega^2\varepsilon_0\mu_0\varepsilon'_r$	$J_m(h_{mn}\alpha)Y_m(h_{mn}b) - Y_m(h_{mn}\alpha)J_m(h_{mn}b) = 0$ $\gamma^2_{mn} = h^2_{mn} - \omega^2\varepsilon_0\mu_0\varepsilon'_r$	$\beta_0 = \omega\sqrt{\varepsilon_0\varepsilon'_r\mu_0}$
Transversal Components	$\underline{e}^{TE}_{mn}(\rho,\varphi) = \frac{j\omega\mu_0}{h'^2_{mn}}(-\frac{\hat\rho}{\rho}\frac{\partial h^{TE}_{z,mn}}{\partial\varphi} + \hat\varphi\frac{\partial h^{TE}_{z,mn}}{\partial\rho})$ $\underline{h}^{TE}_{mn}(\rho,\varphi) = -\frac{\gamma'_{mn}}{h'^2_{mn}}(\hat\rho\frac{\partial h^{TE}_{z,mn}}{\partial\rho} + \hat\varphi\frac{1}{\rho}\frac{\partial h^{TE}_{z,mn}}{\partial\varphi})$	$\underline{e}^{TM}_{mn}(\rho,\varphi) = -\frac{\gamma_{mn}}{h^2_{mn}}(\hat\rho\frac{\partial e^{TM}_{z,mn}}{\partial\rho} + \hat\varphi\frac{1}{\rho}\frac{\partial e^{TM}_{z,mn}}{\partial\varphi})$ $\underline{h}^{TM}_{mn}(\rho,\varphi) = \frac{j\omega\varepsilon_0\varepsilon_r}{h^2_{mn}}(\hat\rho\frac{1}{\rho}\frac{\partial e^{TM}_{z,mn}}{\partial\varphi} - \hat\varphi\frac{\partial e^{TM}_{z,mn}}{\partial\rho})$	$\underline{E}_t = \underline{e}_0(\rho,\varphi)e^{-j\beta_0 z}$ $\underline{H}_t = \underline{h}_0(\rho,\varphi)e^{-j\beta_0 z}$ $\underline{e}_0(\rho,\varphi) = \hat\rho\frac{1}{\rho\ell n(b/\alpha)}$ $\underline{h}_0(\rho,\varphi) = \hat\varphi\frac{1}{\rho\ell n(b/\alpha)}\sqrt{\frac{\varepsilon'_r\varepsilon_0}{\mu_0}}$

the two lines are assumed to be covered by conductive walls. Then, there are no radiation losses in this type of transition.

In the following analysis an $\exp(+j\omega t)$ time dependence of the field quantities is tacitly assumed.

II. Formulation of the Discontinuity Problem

A. Coaxial Line Modes

It is well known that the conventional coaxial line supports transverse electromagnetic (TEM), transverse electric (TE), and transverse magnetic (TM) modes [4], [5]. The electromagnetic fields of the coaxial line modes are given in Table I in an abbreviated form.

Note that in Table I the φ dependence of the longitudinal components is determined from the symmetry considerations with respect to the $x=0$ plane.

The infinite set of TEM, TE_{mn}, and TM_{mn} ($m=0,1,2,\cdots$; $n=1,2,\cdots$) constitutes an orthogonal set of modal field functions on a $z=$ constant plane of the coaxial line. Then the following relations are valid:

$$\iint_{A_C}(\boldsymbol{e}_0\times\boldsymbol{h}_0^*)\cdot\hat z\,dS = C_0 \tag{1}$$

$$\iint_{A_C}(\boldsymbol{e}^{TE}_{mn}\times\boldsymbol{h}^{*TE}_{m'n'})\cdot\hat z\,dS = C^{TE}_{mn}\delta_{mm'}\delta_{nn'} \tag{2}$$

$$\iint_{A_C}(\boldsymbol{e}^{TM}_{mn}\times\boldsymbol{h}^{*TM}_{m'n'})\cdot\hat z\,dS = C^{TM}_{mn}\delta_{mm'}\delta_{nn'} \tag{3}$$

$$\begin{aligned}\iint_{A_C}(\boldsymbol{e}^{TE}_{mn}\times\boldsymbol{h}^{*TM}_{m'n'})\cdot\hat z\,dS &= \iint_{A_C}(\boldsymbol{e}^{TM}_{mn}\times\boldsymbol{h}^{*TE}_{m'n'})\cdot\hat z\,dS\\ &= \iint_{A_C}(\boldsymbol{e}_0\times\boldsymbol{h}^{*TM}_{m'n'})\cdot\hat z\,dS\\ &= \iint_{A_c}(\boldsymbol{e}^{TM}_{mn}\times\boldsymbol{h}_0^*)\cdot\hat z\,dS\\ &= \iint_{A_c}(\boldsymbol{e}_0\times\boldsymbol{h}^{*TE}_{mn})\cdot\hat z\,dS\\ &= \iint_{A_C}(\boldsymbol{e}^{TE}_{mn}\times\boldsymbol{h}_0^*)\cdot\hat z\,dS = 0\end{aligned} \tag{4}$$

where A_C is the cross section of the coaxial line. The mode power coefficients C_0, C^{TE}_{mn}, and C^{TE}_{mn} are computed by substituting expressions from Table I into (1)–(4) and by employing direct integrations over the ρ and φ variables. The expressions for C_0, C^{TE}_{mn}, and C^{TM}_{mn} are given in the Appendix.

B. Computation of the Microstrip Line Mode Characteristics

Because of the partial dielectric filling, only hybrid modes can be guided in the microstrip line region. In the present analysis use is made of the analytical technique developed by Mittra and Itoh [6] to determine the properties of these hybrid modes.

The mode characteristics are determined by computing the nontrivial solutions of the systems

$$\sum_{m=1}^{\infty}\left(\hat{k}_p\delta_{pm}-a_mD_{pm}-M_mk_p\right)\bar{A}_m^{(e)}-\sum_{n=1}^{\infty}\left(b_nD_{pn}+N_nk_p\right)\bar{A}_n^{(h)}=0,\qquad p=1,2,\cdots \quad (5)$$

$$\sum_{m=1}^{\infty}\left(-c_mD_{qm}-X_mk_q\right)\bar{A}_m^{(e)}+\sum_{n=1}^{\infty}\left(\hat{k}_p\delta_{qn}-d_nD_{qn}-Y_nk_q\right)\bar{A}_n^{(h)}=0,\qquad q=1,2,\cdots \quad (6)$$

where $\hat{k}_p=(2n-1)\pi/2L$, δ_{qn} is the Kronecker symbol, and $\bar{A}_m^{(e)}$, $\bar{A}_n^{(h)}$ are the normalized mode expansion coefficients [6]. The coefficients a_m, b_m, c_m, d_m, M_m, N_m, X_m, Y_m, D_{nm}, and k_n are defined in [6] and for an arbitrary order of solution can be computed by using the algorithm described in [7].

Following a well-known procedure [6], [7], the electric and magnetic fields for a specified mode with $\beta=\beta_m$ can be computed by using the relations

$$\boldsymbol{e}_m^{(s)}(\boldsymbol{r})=\left(j\frac{k^2(y)-\beta_m^2}{\beta_m}\psi^{(e)}+\boldsymbol{e}_m(x,y)\right)e^{-j\beta_mz} \quad (7)$$

$$\boldsymbol{h}_m^{(s)}(\boldsymbol{r})=\left(j\frac{k^2(y)-\beta_m^2}{\beta_m}\psi^{(h)}+\boldsymbol{h}_m(x,y)\right)e^{-j\beta_mz},\qquad m=1,2,3,\cdots \quad (8)$$

where

$$k(y)=\begin{cases}k_0\sqrt{\epsilon_r}, & 0<y<d\\ k_0, & d<y<h\end{cases} \quad (9)$$

while the transversal field components $\boldsymbol{e}_m$, $\boldsymbol{h}_m$ and potential functions $\psi^{(e)}$, $\psi^{(h)}$ are given in [7, eqs. (3), (4), (7), and (8)]. Finally the microstrip line being an inhomogeneously dielectric loaded waveguide, the following mode power orthogonality is satisfied [8]:

$$\iint_{A_s}\left(\boldsymbol{e}_m(x,y)\times\boldsymbol{h}_n^*(x,y)\right)\cdot\hat{z}\,dx\,dy=\delta_{mn'}C_m^{(s)} \quad (10)$$

where A_s is the cross-sectional area of the shielded microstrip line. The mode power coefficients $C_m^{(s)}$ ($m=1,2,\cdots$) are computed by direct integrations and are given in the appendix of [7]. In practice only a single mode is allowed to propagate (for $m=1$ in (7) and (8)) on microstrip lines while higher order evanescent waves can appear only near the discontinuity region. In general the mode propagation constants β_m ($m=1,2,\cdots$) could take complex values. However the evanescent waves usually have imaginary propagation constants [7].

III. Mode-Matching Procedure

In order to determine the frequency-dependent characteristics of the coaxial to microstrip transition, an incident TEM wave propagating parallel to the positive z axis is taken inside the coaxial line (see Fig. 1). Then the transversal $\boldsymbol{E}_t-\boldsymbol{H}_t$ fields inside the coaxial line ($z<0$ half space) region can be expressed as a superposition of the incident TEM wave plus an infinite sum of all the reflected waves:

$$\boldsymbol{E}_t(\rho,\varphi,z)=\boldsymbol{e}_0(\rho,\varphi)\,e^{-j\beta_0z}+A_0\boldsymbol{e}_0(\rho,\varphi)\,e^{j\beta_0z}+\sum_{m,n}\left(B_{mn}\boldsymbol{e}_{mn}^{\mathrm{TE}}e^{\gamma'_{mn}z}+\Gamma_{mn}\boldsymbol{e}_{mn}^{\mathrm{TM}}e^{\gamma_{mn}z}\right) \quad (11)$$

$$\boldsymbol{H}_t(\rho,\varphi,z)=\boldsymbol{h}_0(\rho,\varphi)\,e^{-j\beta_0z}-A_0\boldsymbol{h}_0(\rho,\varphi)\,e^{j\beta_0z}-\sum_{m,n}\left(B_{mn}\boldsymbol{h}_{mn}^{\mathrm{TE}}e^{\gamma'_{mn}z}+\Gamma_{mn}\boldsymbol{h}_{mn}^{\mathrm{TM}}e^{\gamma_{mn}z}\right) \quad (12)$$

where $\sum_{m,n}=\sum_{m=0}^{\infty}\sum_{n=1}^{\infty}$ and A_0, B_{mn}, Γ_{mn} ($m=0,1,2,\cdots$; $n=1,2,\cdots$) are unknown coefficients to be determined. The corresponding transversal field components inside the $z>0$ semi-infinite microstrip line region can be written as follows:

$$\boldsymbol{E}_t'(x,y,z)=\sum_{k=1}^{\infty}D_k\boldsymbol{e}_k(x,y)\,e^{-j\beta_kz} \quad (13)$$

$$\boldsymbol{H}_t'(x,y,z)=\sum_{k=1}^{\infty}D_k\boldsymbol{e}_k(x,y)\,e^{-j\beta_kz} \quad (14)$$

where D_k ($k=1,2,\cdots$) again are unknown coefficients to be determined.

On applying the boundary condition on the $z=0$ plane for the continuity of the transversal electric and magnetic field components, the following equations are obtained:

$$\sum_{k=1}^{\infty}D_k\boldsymbol{e}_k(x,y)=\begin{cases}0 & \text{for } (x,y)\notin A_c\\ \boldsymbol{e}_0(\rho,\varphi)+A_0\boldsymbol{e}_0(\rho,\varphi)+\sum_{m,n}\left(B_{mn}\boldsymbol{e}_{mn}^{\mathrm{TE}}(\rho,\varphi)+\Gamma_{mn}\boldsymbol{e}_{mn}^{\mathrm{TM}}(\rho,\varphi)\right) & \text{for } (x,y)\in A_c\end{cases} \quad (15)$$

$$\boldsymbol{h}_0(\rho,\varphi)-A_0\boldsymbol{h}_0(\rho,\varphi)-\sum_{m,n}B_{mn}\boldsymbol{h}_{mn}^{\mathrm{TE}}(\rho,\varphi)-\sum_{m,n}\Gamma_{mn}\boldsymbol{h}_{mn}^{\mathrm{TM}}(\rho,\varphi)=\sum_{k=1}^{+\infty}D_k\boldsymbol{h}_k(x,y)\qquad \text{for } (x,y)\in A_c \quad (16)$$

where A_c is the coaxial line cross section. In order to determine the unknown A_0, B_{mn}, Γ_{mn}, and D_n coefficients it is proposed to take the vector products of (15) with $h_l^*(x,y)$ and of (16) with $\boldsymbol{e}_0^*$, $\boldsymbol{e}_{\mu\nu}^{*\mathrm{TE}}$, and $\boldsymbol{e}_{\mu\nu}^{*\mathrm{TM}}$ respectively. Then by integrating the vector product of (16) over the cross section A_c of the coaxial line because of the orthogonality relations given in (1)–(4), the unknown coefficients A_0, B_{mn}, and Γ_{mn} can be expressed in terms of the

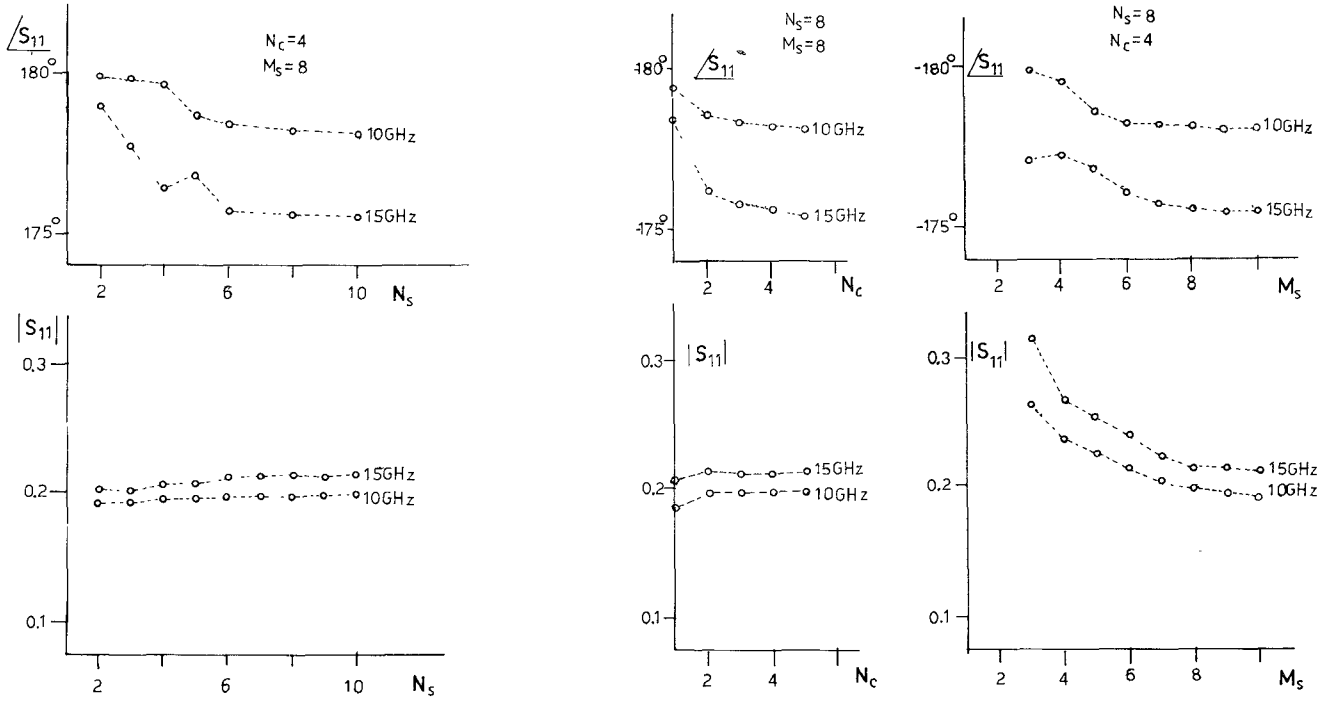

Fig. 2. Convergence patterns of the S_{11} reflection coefficient with N_s (number of modes of microstrip taken into account), N_c (number of modes of coaxial line taken into account), and M_s (truncation order taken into account to compute the microstrip mode field distributions). Here $a = 0.200$ mm, $b = 0.600$ mm, $\epsilon_r = 10$, $w = 0.300$ mm, $d = 0.635$ mm, $2L = 9.52$ mm, $h = 6.35$ mm, and $\epsilon_r' = 2.32$.

D_k coefficients as follows:

$$A_0 = 1 - \sum_{k=1}^{+\infty} D_k \frac{X_k^*}{C_0^*} \tag{17}$$

$$B_{mn} = -\sum_{k=1}^{\infty} D_k \frac{Y_{k,mn}^*}{C_{mn}^{*TE}} \tag{18}$$

$$\Gamma_{mn} = -\sum_{k=1}^{\infty} D_k \frac{Z_{k,mn}^*}{C_{mn}^{*TM}} \tag{19}$$

where C_0, C_{mn}^{TE}, and C_{mn}^{TM} are as defined in (1)–(4) and

$$X_k = \iint_{A_c} (\boldsymbol{e}_0 \times \boldsymbol{h}_k^*) \cdot \hat{z}\, dx\, dy \tag{20}$$

$$Y_{k,mn} = \iint_{A_c} (\boldsymbol{e}_{mn}^{\mathrm{TE}} \times \boldsymbol{h}_k^*) \cdot \hat{z}\, dx\, dy \tag{21}$$

$$Z_{k,mn} = \iint_{A_c} (\boldsymbol{e}_{mn}^{\mathrm{TM}} \times \boldsymbol{h}_k^*) \cdot \hat{z}\, dx\, dy. \tag{22}$$

The values of the coupling coefficients X_k, $Y_{k,mn}$, and $Z_{k,mn}$ are computed analytically and are given in the Appendix. Substituting (17)–(19) into (15), then taking the vector product with $\boldsymbol{h}_l^*(x, y)$ and integrating the z component of this equation on the A_c area (see Fig. 1), it is found that

$$\sum_{p=1}^{\infty} D_p \left\{ \frac{X_l X_p^*}{C_0^*} + \sum_{m,n} \frac{Y_{l,mn} Y_{p,mn}^*}{C_{mn}^{*\mathrm{TE}}} + \sum_{m,n} \frac{Z_{l,mn} Z_{p,mn}^*}{C_{mn}^{*\mathrm{TM}}} + \left(\delta_{lp} C_p^{(s)} - C_{l_p}^{(s)} \right) \right\} = 2X_l \qquad (l = 1, 2, \cdots) \tag{23}$$

where

$$C_{lp}^{(s)} = \iint_{(A_s - A_c)} \left(\boldsymbol{e}_p(x, y) \times \boldsymbol{h}_l^*(x, y) \right) \cdot \hat{z} \, dx\, dy \tag{24}$$

and $(A_s - A_c)$ is the microstrip line cross section area excluding the coaxial line cross section area (see Fig. 1). The coefficients $C_p^{(s)}$ are as defined in (10). The numerical values of the $C_{lp}^{(s)}$ coefficients are determined by applying a direct numerical integration procedure in the x, y plane.

As a final step, again the vector product of (15) is taken with $h_l^*(x, y)$, and the $\hat{z}$ component of it is integrated over the $(A_s - A_c)$ area. Then it is found that

$$\sum_{p=1}^{\infty} D_p C_{lp}^{(s)} = 0 \qquad (l = 1, 2, \cdots) \tag{25}$$

should also be satisfied in conjunction with the infinite set of equations (23).

It is important to emphasize that the infinite sets given by (23) and (25) are complementary to each other, and in truncating them into finite summations care should be taken to satisfy properly the boundary conditions on the A_c and $(A_s - A_c)$ cross-sectional areas (see Fig. 1) as these are described by (15). To this end if N_s is the number of microstrip models taken into account and N_{s1} and N_{s2} are the numbers of equations taken from the systems (23) and (24), respectively, it should be that $N_s = N_{s1} + N_{s2}$. However it is not clear initially which are the most appropriate subsets of equations to be chosen from the two infinite systems of equations. In order to determine the best choice of N_{s1}, N_{s2} values the physical picture of microstrip modes and of the associated scattering phenomenon should be

investigated. Examination of the mode field distributions shows that the dominant propagating-mode (known as the quasi-static mode) power density is most concentrated under the printed line, while the high-order evanescent-mode field distributions are widely spread on the shielded microstrip line cross section. Therefore it is suitable to solve (23) for low-order modes and then employ high-order modes to satisfy (25). Numerical computations revealed that the simplest and most efficient approach is to employ $N_{s1}=1$ and $N_{s2}=N_s-1$. This means that in (25) the evanescent-mode coefficients $D_2, D_3, \cdots, D_{N_s}$ are determined in terms of the dominant-mode expansion coefficient D_1. On substituting the values of $D_2, D_3, \cdots, D_{N_s}$ into (23), an equation giving the numerical value of D_1 is obtained which can be solved by numerical techniques. Furthermore it is found that this algorithm provides almost the same numerical values if, instead of $N_{s1}=1$, selections such as $N_{s2}=2$ and $N_{s1}=3$ are employed provided that $N_{s1} \ll N_s$ and of course that the high-order mode coefficients are taken as unknowns in (25).

Convergence properties of the computed results are examined to estimate the required number of higher order modes on both transmission lines, as will be shown in Section IV. Assuming the D_l ($l=1,2,\cdots$) coefficients are known, then the reflected TEM wave expansion coefficient A_0 is computed easily by using (17), giving the desired reflection coefficient value.

IV. Numerical Computations and Discussion

Numerical computations have been performed for several coaxial to microstrip line transition geometries by applying the theory developed in the previous sections. In each case extensive convergence tests by increasing the number of modes on both sides of the transition have been performed. In Fig. 2 sample convergence patterns are presented at two microwave frequencies varying the following integers:

N_s = number of modes on microstrip line,
N_c = number of modes on coaxial line,
M_s = number of terms taken into account to compute the microstrip mode field distributions (see (5), (6), and [6]).

Numerical computations showed that for ordinary coaxial and microstrip line dimensions six to eight modes on both lines were sufficient to provide satisfactory convergence. The value $M_s=10$ was found to provide satisfactory accuracy for the range of parameters examined in this paper. Furthermore the relative convergence properties of the mode-matching solutions by using different N_s/N_c ratios have also been examined. It is found that there is no significant effect on the convergence in taking nonequal numbers of modes on the two sides of the discontinuity and mostly $N_s=N_c$ is employed in the course of the computations.

In presenting the numerical results the conventional S parameters will be employed. To this end the coaxial and microstrip lines are defined as the number 1 and 2 ports of

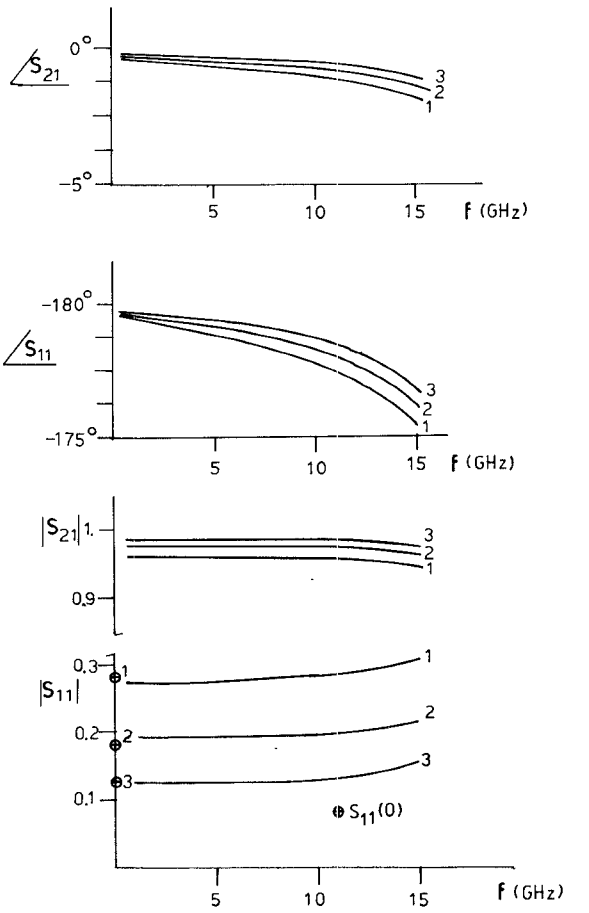

Fig. 3. Variation of $|S_{11}|$, $|S_{21}|$, $\angle S_{11}$, and $\angle S_{21}$ with frequency for several coaxial line dimensions:

1) $a=0.250$ mm, $b=0.600$ mm, $\epsilon_r'=2.32$
2) $a=0.200$ mm, $b=0.600$ mm, $\epsilon_r'=2.32$
3) $a=0.175$ mm, $b=0.600$ mm, $\epsilon_r'=2.32$.

The microstrip line dimensions are the same as those in Fig. 2.

the transition two-port network. Then on using as a reference impedance the wave impedance of the coaxial line, the S parameters are defined as

$$S_{11}=-A_0 \qquad S_{21}=S_{12}=-D_1\sqrt{\frac{C_1^{(s)}}{C_0}}. \tag{26}$$

Notice that the minus sign in front of S_{11} and S_{21} is introduced because the dominant modal field expression ($m=1$) given in (7) and (8) is computed with $A_1^{(h)}=1$ (for details, see [7]) and this corresponds to a quasi-TEM field distribution in which the microstrip line is in negative potential with respect to the ground plane. Because of the lossless transition the value of S_{22} can be computed easily in terms of the S_{11} and S_{21} parameter values [9]. Furthermore the validity of the power conservation theorem expressed by the equation

$$|S_{11}|^2+|S_{12}|^2=1$$

is verified in each case. It is found that this condition is satisfied with an accuracy of 5‰ by using $N_c=N_s=8$ for

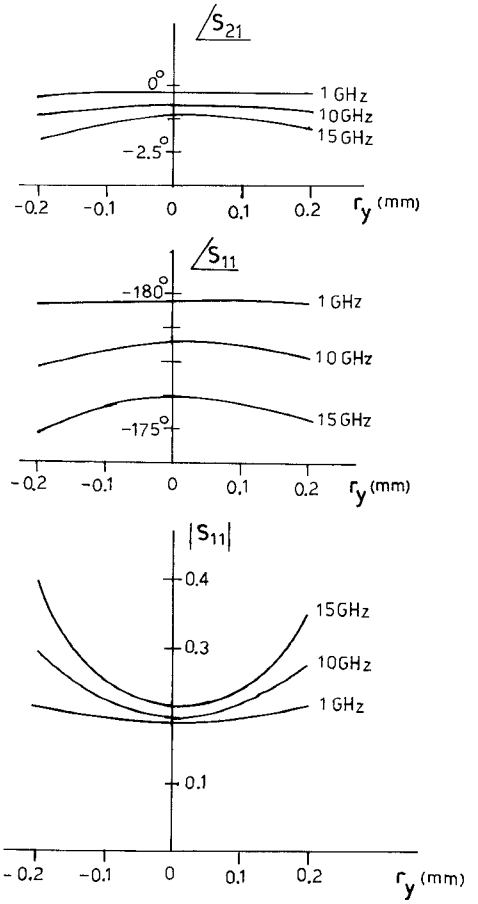

Fig. 4. Variation of $|S_{11}|$, $\angle S_{11}$, and $\angle S_{21}$ with r_y (see Fig. 1) for $\alpha = 0.200$ mm, $b = 0.600$ mm, and $\epsilon_r' = 2.32$. The microstrip line dimensions are the same as in Fig. 2.

the microstrip and coaxial line dimensions given in the following.

In all the computed results the coaxial line dielectric is assumed to be polyethylene with $\epsilon_r' = 2.32$ and the b/a ratios are taken such that the characteristic impedances Z_0 are close to 50 Ω.

The microstrip line substrate is taken to be alumina ($\epsilon_r = 10$). The shielding box dimensions (see Fig. 1) are taken to be $2L = 9.52$ mm and $h = 6.35$ mm. The microstrip line substrate thickness is always $d = 0.635$ mm. The w/d ratio is also taken such that the quasi-static TEM microstrip mode characteristic impedance is close to 50 Ω.

In Fig. 3 results are presented for the frequency dependence of the scattering parameters of microstrip to coaxial transition for three different coaxial line dimensions. On the same figures the transmission line theory $S_{11}(0) = (Z_{0s} - Z_{0c})/(Z_{0s} + Z_{0c})$ values are also shown, where Z_{0c} and Z_{0s} are the TEM wave characteristic impedances of the coaxial and the shielded microstrip line, respectively. The numerical values of the Z_{0s} quasi-static characteristic impedances are computed by using the results given in [10] while $Z_{0c} = 60 \cdot \ln(b/\alpha)/\sqrt{\epsilon_r'}$ (Ω). The coincidence of the rigorous solutions at low frequencies with the transmission line theory values is noticed. This agreement verifies the correctness of the present solutions. Furthermore it is noticeable that the frequency dependence of the S parameters starts at quite low frequencies (about 5 GHz).

In Fig. 4 results are quoted for the dependence of the S parameters on the r_y distance between the coaxial line axis and the microstrip line surface (see Fig. 1) at frequencies of 1, 10, and 15 GHz. The rather strong dependence of the reflection coefficient $|S_{11}|$ on the r_y displacement, especially at high frequencies, is noticed.

V. Conclusions

A rigorous approach has been presented for the analysis of a coaxial to shielded microstrip line transition. The boundary conditions on the transition plane are satisfied by employing a modified mode-matching technique. This technique can be applied to different types of transition problems in microwave circuits. Numerical results are presented for several coaxial to shielded microstrip line transitions and useful results are presented for the frequency dependence of this type of transition. The theory presented here can be used in connector design and in compensating the transition mismatch impedances in coaxial to microstrip transitions.

Appendix
Computation of the C_0, C_{mn}^{TE}, and C_{mn}^{TM} Coefficients

The coefficients C_0, C_{mn}^{TE}, and C_{mn}^{TM} defined in (1)–(4) are given as follows:

$$C_0 = 2\pi \sqrt{\frac{\epsilon_0 \epsilon_r'}{\mu_0}} \frac{1}{\ln(b/\alpha)}$$

$$C_{mn}^{TM} = -\frac{j\omega \epsilon_0 \epsilon_r' V_{mn}'}{h_{mn}'^2} \pi \left(I_1 + I_2 \cdot x^2 - 2I_3 x\right) \cdot \epsilon_m$$

and

$$C_{mn}^{TE} = \frac{j\omega \mu_0 V_{mn}}{h_{mn}^2} \pi \left(I_1 + I_2 x'^2 - 2I_3 x'\right)$$

where

$$\epsilon_m = \begin{cases} 2 & \text{when } m = 0 \\ 1 & \text{elsewhere} \end{cases}$$

$$x = \frac{J_m(h\alpha)}{Y_m(h\alpha)} \qquad x' = \frac{J_m'(h\alpha)}{Y_m'(h\alpha)}$$

$$I_1 = J_m(hb) J_m'(hb) \frac{b}{h} - J_m(h\alpha) J_m'(h\alpha) \frac{\alpha}{h} + \frac{b^2}{2}\left(J_m^2(hb) - J_{m+1}(hb) J_{m-1}(hb)\right) - \frac{\alpha^2}{2}\left(J_m^2(h\alpha) - J_{m+1}(h\alpha) J_{m-1}(h\alpha)\right)$$

$$I_2 = Y_m(hb) Y_m'(hb) \frac{b}{h} - Y_m(h\alpha) Y_m'(h\alpha) \frac{\alpha}{h} + \frac{b^2}{2}\left(Y_m^2(hb) - Y_{m+1}(hb) Y_{m-1}(hb)\right) - \frac{\alpha^2}{2}\left(Y_m^2(h\alpha) - Y_{m+1}(h\alpha) Y_{m-1}(h\alpha)\right)$$

$$I_3 = J_m(hb)Y_m'(hb)\frac{b}{h} - J_m(h\alpha)Y_m'(h\alpha)\frac{\alpha}{h} + \frac{1}{h^2}\int_{h\alpha}^{hb} J_m(z)Y_m(z)\,z\,dz$$

with

$$h = \begin{cases} h_{mn} & \text{for TM modes} \\ h'_{mn} & \text{for TE modes.} \end{cases}$$

Computation of the X_k, $Y_{k,nm}$, and $Z_{k,nm}$ Terms

The coefficients X_k, $Y_{k,nm}$, and $Z_{k,nm}$ defined in (20)–(22) can be expressed with the following general formula:

$$C = A\cdot\left\{\sum_{l=1}^{\infty}\left(-\frac{\omega_0\epsilon_0\epsilon_r}{\beta_k^*}A_l^{*(e)}\hat{k}_l + A_l^{*(h)}a_l^{*(1)}\right)\cdot I_1 - \sum_{l=1}^{\infty}\left(-\frac{\omega\epsilon_0\epsilon_r}{\beta_k^*}A_l^{*(e)}a_l^{*(1)} + A_l^{*(h)}\hat{k}_l\right)\cdot I_2 + \sum_{l=1}^{\infty}\left(-\frac{\omega\epsilon_0}{\beta_k^*}B_l^{*(e)}\hat{k}_l - B_l^{*(h)}a_l^{*(2)}\right)\cdot I_3 - \sum_{l=1}^{\infty}\left(\frac{\omega\epsilon_0}{\beta_k^*}B_l^{*(e)}a_l^{*(2)} + B_l^{*(h)}\hat{k}_l\right)\cdot I_4\right\}$$

where $C = X_k$ or $Y_{k,nm}$ or $Z_{k,nm}$. The $a_l^{(1)}$, $a_l^{(2)}$, and $\hat{k}_l$ are defined in the appendix of [7] and the terms A, I_1, I_2, I_3, and I_4 are quoted separately for each coefficient case (X_k, $Y_{k,nm}$ and $Z_{k,nm}$) in the following:

X_k Coefficients:

$$A = \frac{1}{\ln(b/a)}$$

$$I_1 = \iint_{A_c}\sinh a_l^{*(1)}y\sin\hat{k}_l x\frac{\cos\varphi}{\rho}\,dx\,dy$$

$$I_2 = \iint_{A_c}\cosh a_l^{*(1)}y\cos\hat{k}_l x\frac{\sin\varphi}{\rho}\,dx\,dy$$

$$I_3 = \iint_{A_c}\sinh a_l^{*(2)}(h-y)\sin\hat{k}_l x\frac{\cos\varphi}{\rho}\,dx\,dy$$

$$I_4 = \iint_{A_c}\cosh a_l^{*(2)}(h-y)\cos\hat{k}_l x\frac{\sin\varphi}{\rho}\,dx\,dy.$$

$Z_{k,nm}$ Coefficients:

$$A = -v/h$$

$$I_1 = \iint_{A_c}\sinh a_l^{*(1)}y\sin\hat{k}_l x\cdot\left\{-\sin\varphi\frac{m}{h\rho}\left(J_m(h\rho) - \frac{J_m(h\alpha)}{Y_m(h\alpha)}Y_m(h\rho)\right)\cdot f_1(m,\varphi) + \cos\varphi\left(J_m'(h\rho) - \frac{J_m(h\alpha)}{Y_m(h\alpha)}Y_m'(h\rho)\right)\cdot f_2(m,\varphi)\right\}dx\,dy$$

$$I_2 = \iint_{A_c}\cosh a_l^{*(1)}y\cos\hat{k}_l x\cdot\left\{\cos\varphi\frac{m}{h\rho}\left(J_m(h\rho) - \frac{J_m(h\alpha)}{Y_m(h\alpha)}Y_m(h\rho)\right)\cdot f_1(m,\varphi) + \sin\varphi\left(J_m'(h\rho) - \frac{J_m(h\alpha)}{Y_m(h\alpha)}Y_m'(h\rho)\right)\cdot f_2(m,\varphi)\right\}dx\,dy$$

$$I_3 = \iint_{A_c}\sinh a_l^{*(2)}(h-y)\sin\hat{k}_l x\cdot\left\{-\sin\varphi\frac{m}{h\rho}\left(J_m(h\rho) - \frac{J_m(h\alpha)}{Y_m(h\alpha)}Y_m(h\rho)\right)\cdot f_1(m,\varphi) + \cos\varphi\left(J_m'(h\rho) - \frac{J_m(h\alpha)}{Y_m(h\alpha)}Y_m'(h\rho)\right)\cdot f_2(m,\varphi)\right\}dx\,dy$$

$$I_4 = \iint_{A_c}\cosh a_l^{*(2)}(h-y)\cos\hat{k}_l x\cdot\left\{\cos\varphi\frac{m}{h\rho}\left(J_m(h\rho) - \frac{J_m(h\alpha)}{Y_m(h\alpha)}Y_m(h\rho)\right)\cdot f_1(m,\varphi) + \sin\varphi\left(J_m'(h\rho) - \frac{J_m(h\alpha)}{Y_m(h\alpha)}Y_m'(h\rho)\right)\cdot f_2(m,\varphi)\right\}dx\,dy$$

and

$$f_1(m,\varphi) = \begin{cases} -\sin m\varphi, & m = \text{even} \\ \cos m\varphi, & m = \text{odd} \end{cases}$$

$$f_2(m,\varphi) = \begin{cases} \cos m\varphi, & m = \text{even} \\ \sin m\varphi, & m = \text{odd.} \end{cases}$$

$Y_{k,nm}$ Coefficients:

$$A = \frac{j\omega\mu_0}{h}$$

$$I_1 = \iint_{A_c}\sinh a_l^{*(1)}y\sin\hat{k}_l x\cdot\left\{-\sin\varphi\left(J_m'(h\rho) - \frac{J_m'(h\alpha)}{Y_m'(h\alpha)}Y_m'(h\rho)\right)\cdot f_1(m,\varphi) + \cos\varphi\frac{m}{h\rho}\left(J_m(h\rho) - \frac{J_m'(h\alpha)}{Y_m'(h\alpha)}Y_m(h\rho)\right)\cdot f_2(m,\varphi)\right\}dx\,dy$$

$$I_2 = \iint_{A_c}\cosh a_l^{*(1)}y\cos\hat{k}_l x\cdot\left\{\cos\varphi\left(J_m'(h\rho) - \frac{J_m'(h\alpha)}{Y_m'(h\alpha)}Y_m'(h\rho)\right)\cdot f_1(m,\varphi) + \sin\varphi\frac{m}{h\rho}\left(J_m(h\rho) - \frac{J_m'(h\alpha)}{Y_m'(h\alpha)}Y_m(h\rho)\right)\cdot f_2(m,\varphi)\right\}dx\,dy$$

$$I_3 = \iint_{A_c}\sinh a_l^{*(2)}(h-y)\sin\hat{k}_l x\cdot\left\{-\sin\varphi\left(J_m'(h\rho) - \frac{J_m'(h\alpha)}{Y_m'(h\alpha)}Y_m'(h\rho)\right)\cdot f_1(m,\varphi) + \cos\varphi\frac{m}{h\rho}\left(J_m(h\rho) - \frac{J_m'(h\alpha)}{Y_m'(h\alpha)}Y_m(h\rho)\right)\cdot f_2(m,\varphi)\right\}dx\,dy$$

$$I_4 = \iint_{A_c} \cosh a_l^{*(2)}(h-y)\cos \hat{k}_l x \cdot \left\{ \cos\varphi \left(J_m'(h\rho) - \frac{J_m'(h\alpha)}{Y_m'(h\alpha)} Y_m'(h\rho) \right) \cdot f_1(m,\varphi) + \sin\varphi \frac{m}{h\rho} \left(J_m(h\rho) - \frac{J_m'(h\alpha)}{Y_m'(h\alpha)} Y_m(h\rho) \right) \cdot f_2(m,\varphi) \right\} dx\,dy$$

and

$$f_1(m,\varphi) = \begin{cases} \sin m\varphi, & m = \text{even} \\ \cos m\varphi, & m = \text{odd} \end{cases}$$

$$f_2(m,\varphi) = \begin{cases} -\cos m\varphi, & m = \text{even} \\ \sin m\varphi, & m = \text{odd}. \end{cases}$$

In computing the integrals over the A_c intersection area (see Fig. 1) a direct two-dimensional numerical integral procedure is employed. To this end a 12-point multisegment Gauss quadrature is utilized.

References

[1] W. Schminke, "Reflexionen am Übergang einer Koaxialleitung auf eine Streifenleitung," *Arch. Elek. Übertragung.*, Band 33, pp. 6–12, 1979.

[2] T. C. Edwards, *Foundations for Microstrip Circuit Design*. New York: Wiley, 1984, pp. 174–176.

[3] E. H. England, "A coaxial to microstrip transition," *IEEE Trans. Microwave Theory Tech.*, vol. MTT-26, pp. 47–48, 1976.

[4] D. S. Jones, *The Theory of Electromagnetism*. Oxford: Pergamon Press, 1964, ch. 5.

[5] N. Marcuvitz, *Waveguide Handbook*. New York: Dover, 1965, ch. 2.

[6] R. Mittra and T. Itoh, "A new technique for the analysis of the dispersion characteristics of microstrip lines," *IEEE Trans. Microwave Theory Tech.*, vol. MTT-19, pp. 47–56, 1971.

[7] N. K. Uzunoglu, C. N. Capsalis, and C. P. Chronopoulos, "Frequency dependent analysis of a shielded microstrip step discontinuity using an efficient mode matching technique," *IEEE Trans. Microwave Theory Tech.*, to be published.

[8] R. E. Collin, *Field Theory of Guided Waves*. New York: McGraw-Hill, 1960, ch. 6.

[9] R. E. Collin, *Foundations for Microwave Engineering*. New York: McGraw-Hill, 1965, sec. 4.8.

[10] H. A. Wheeler, "Transmission-line properties of parallel wide strips by a conformal mapping approximation," *IEEE Trans. Microwave Theory Tech.*, vol. MTT-12, pp. 280–289, May 1964.

Christos N. Capsalis was born in Nafplion, Greece, on September 25, 1956. He received the Diploma of E.E. and M.E. from the National Technical University of Athems (NTUA), Athens, Greece, in 1979 and the bachelor's degree in economics from the University of Athens, Athens, Greece, in 1983. He also received the Ph.D. degree in electrical engineering from NTUA in 1985.

Since January 1982, he has been a Research Associate in the Department of Electrical Engineering at NTUA. In November 1986 he was elected Lecturer at NTUA, the position that he currently holds. His main research interests are in the electromagnetic field area, with emphasis on scattering and propagation at millimeter and optical wavelengths.

✠

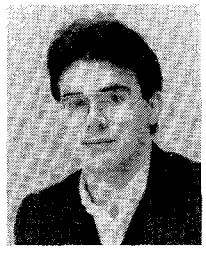

Constantinos P. Chronopoulos was born in Tripolis, Greece, in 1964. He received the Diploma in electrical engineering from the National Technical University of Athens (NTUA), Athens, Greece, in 1986. Since then, he has been working at NTUA toward the Ph.D. degree with a scholarship from the Bodosakis Foundation. His thesis deals with microstrip discontinuities. His research interests include fiber optics and millimeter-wave applications.

✠

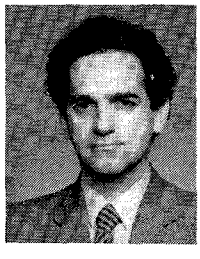

Nikolaos K. Uzunoglu (M'82) received the B.Sc. degree in electronics engineering from the Istanbul Technical University, Turkey, in 1973. He obtained the M.Sc. and Ph.D. degrees from the University of Essex, England, in 1974 and 1976, respectively.

He worked for the Hellenic Navy Research and Technology Development Office from 1977 to 1984. During this period, he also worked, on a part-time basis, at the National Technical University of Athens, Athens, Greece, on electromagnetic theory. In 1984 he was elected Associate Professor at the National Technical University of Athens and in 1988 he was named Professor, the position he holds presently. He served as Associate Chairman of the Department of Electrical University for the years 1986–1988. In 1988 he was elected Chairman of the department for the 1988–1990 academic years. His research interests are microwave applications in telecommunications and medicine, fiber-optic components, and electromagnetic theory.